Frontiers of Information Technology & Electronic Engineering
www.jzus.zju.edu.cn; engineering.cae.cn; www.springerlink.com
ISSN 2095-9184 (print); ISSN 2095-9230 (online)
E-mail: jzus@zju.edu.cn

Dynamic analysis, FPGA implementation, and cryptographic application of an autonomous 5D chaotic system with offset boosting

Sifeu TAKOUGANG KINGNI[†‡1], Karthikeyan RAJAGOPAL[2], Serdar ÇIÇEK[3], Ashokkumar SRINIVASAN[4], Anitha KARTHIKEYAN[2]

[1]*Department of Mechanical, Petroleum and Gas Engineering, Faculty of Mines and Petroleum Industries, The University of Maroua, Maroua P.O. Box 46, Cameroon*

[2]*Faculty of Electrical and Electronics Engineering, Ton Duc Thang University, Ho Chi Minh City 758307, Vietnam*

[3]*Department of Electronic and Automation, Vocational School of Hacıbektaş, Nevşehir Hacıbektaş Veli University, Hacıbektaş 50800, Turkey*

[4]*Center for Nonlinear Dynamics, Defence University, Bishoftu 6020, Ethiopia*

[†]E-mail: stkingni@gmail.com

Received Mar. 26, 2019; Revision accepted May 25, 2019; Crosschecked May 7, 2020

Abstract: An autonomous five-dimensional (5D) system with offset boosting is constructed by modifying the well-known three-dimensional autonomous Liu and Chen system. Equilibrium points of the proposed autonomous 5D system are found and its stability is analyzed. The proposed system includes Hopf bifurcation, periodic attractors, quasi-periodic attractors, a one-scroll chaotic attractor, a double-scroll chaotic attractor, coexisting attractors, the bistability phenomenon, offset boosting with partial amplitude control, reverse period-doubling, and an intermittency route to chaos. Using a field programmable gate array (FPGA), the proposed autonomous 5D system is implemented and the phase portraits are presented to check the numerical simulation results. The chaotic attractors and coexistence of the attractors generated by the FPGA implementation of the proposed system have good qualitative agreement with those found during the numerical simulation. Finally, a sound data encryption and communication system based on the proposed autonomous 5D chaotic system is designed and illustrated through a numerical example.

Key words: Chaotic system; Hopf bifurcation; Coexistence of attractors; Offset boosting; FPGA implementation; Sound encryption

https://doi.org/10.1631/FITEE.1900167 **CLC number:** TN79

1 Introduction

Chaotic systems have been used in many fields of science because they have features such as aperiodic behavior, randomness, prediction difficulty, and extreme sensitivity to initial conditions and parameter values (Hou et al., 2012; Li CQ et al., 2018a). To take advantages of the features of chaotic systems, it is important to apply these systems in engineering applications. Chaos theory has advanced development in many fields since the chaotic attractor was first found in 1963 by Lorentz. Hyperchaotic systems have more complex dynamical behaviors than ordinary chaotic systems. This complexity implies that hyperchaos has more than enough value in engineering applications. From hyperchaotic systems, such as the Rössler system (Rössler, 1979), the Chen system (Li X, 2009), and many other systems (Jia, 2007; Wang JH et al., 2008; Vaidyanathan, 2013), it can be understood that higher-dimensional systems have more complex dynamics. In the n-dimensional ($n\geq 4$) system (Thamilmaran et al, 2004; Li YX et al., 2005; Qi et al., 2008; Wang XY and Wang, 2008; Yang and Liu,

‡ Corresponding author
ORCID: Sifeu TAKOUGANG KINGNI, http://orcid.org/0000-0003-1547-6856

2009; Yang et al., 2009; Shen et al., 2014; Chen YM and Yang, 2015; Li QD et al., 2015), hyperchaos can happen and is characterized by more than one positive Lyapunov exponent. Therefore, it is worthy to study high-dimensional hyperchaotic systems with a corresponding number of positive Lyapunov exponents. In nonlinear science, the hyperchaos theory has become a dominant topic. Due to its characteristics of high capacity, high security, and high efficiency, it has been applied in nonlinear circuits, secure communication, lasers, neural networks, and so on. In practice, for each new system, either the chaos or the hyperchaos imposes anomalous technical requirements.

Studies on autonomous five-dimensional (5D) systems have focused mainly on the generation of hyperchaos (Hu, 2009; Yang and Chen, 2013; Rech, 2014; Ojoniyi and Njah, 2016; Wei et al., 2017; Singh et al., 2018). Some researchers have focused on the synchronization and control of 5D systems (Wei et al., 2018). This topic has motivated us to perform analysis and field programmable gate array (FPGA) implementation of an autonomous 5D chaotic system with offset boosting and apply it to sound encryption design. After analyzing the dynamics of the proposed system, the system is implemented in an FPGA to demonstrate that realization of the system is possible with hardware since FPGA implementation is suitable for complex systems (Rajagopal et al., 2017c). The development of technology has made digital hardware implementation less expensive, faster, and easier to design. FPGA is an efficient platform for implementing substantial high-quality, high-throughput approximations for higher-order systems that are less costly and require less time.

2 Analysis of the proposed autonomous 5D system with offset boosting

Consider the autonomous three-dimensional (3D) system proposed by Liu and Chen (2004):

$$\begin{cases}\dot{x}=ax-yz,\\ \dot{y}=-by+xz,\\ \dot{z}=-cz+xy,\end{cases} \tag{1}$$

where x, y, and z are state variables, and a, b, and c are positive parameters. Liu and Chen (2004) have shown that system (1) has five equilibrium points which are all unstable if $a<b+c$. System (1) has a double-scroll chaotic attractor for (a, b, c)=(3, 10, 6) and a four-scroll chaotic attractor for (a, b, c)=(1, 20, 12). Two additional state variables w and u are added to system (1) to obtain an autonomous 5D system:

$$\begin{cases}\dot{x}=ax-yz-u,\\ \dot{y}=-by+xz-zw,\\ \dot{z}=-cz+xy,\\ \dot{w}=d(y-w),\\ \dot{u}=ex+s,\end{cases} \tag{2}$$

where d, e, and s are positive parameters. System (2) is constructed not by the extension of the existing 4D nonlinear systems as the majority of 5D systems, but by modifying the interesting 3D Liu and Chen system. System (2) is dissipative if $a-b-c-d<0$. System (2) has only one equilibrium point $O(0, 0, 0, 0, 0)$ for $s=0$. When $c\neq0$, $e\neq0$, and $s\neq0$, it has two equilibrium points: $E_1(-s/e,\ 0,\ 0,\ 0,\ -as/e)$ and $E_2(-s/e,\ (bce^2-s^2)/(es),\ (s^2-bce^2)/(es^2),\ (bce^2-s^2)/(es),\ [(bce^2-s^2)^2-ace^2s^2]/(cse^3)$. The characteristic equation of system (2) evaluated at the equilibrium point O is expressed as

$$\lambda^5+\delta_1\lambda^4+\delta_2\lambda^3+\delta_3\lambda^2+\delta_4\lambda+\delta_5=0, \tag{3}$$

where

$$\begin{cases}\delta_1=-a+b+c+d,\\ \delta_2=e+cd+bd+bc-ad-ac-ab,\\ \delta_3=be+ce+de+bcd-abc-abd-acd,\\ \delta_4=bce+bde+cde-abcd,\\ \delta_5=bcde.\end{cases} \tag{4}$$

Using the Routh-Hurwitz conditions, Eq. (3) has all roots with negative real parts if and only if

$$\begin{cases}\delta_i>0,\ \ i=1, 2, ..., 5,\\ (\delta_1\delta_4-\delta_5)(\delta_1\delta_2\delta_3-\delta_3^2-\delta_1^2\delta_4)\\ \qquad>\delta_5(\delta_1\delta_2-\delta_3)^2+\delta_1\delta_5^2,\\ \delta_1\delta_2\delta_3>\delta_3^2+\delta_1^2\delta_4.\end{cases} \tag{5}$$

The characteristic equation of system (2) evaluated at the equilibrium point E_1 is expressed as

$$\lambda^5+\delta_{11}\lambda^4+\delta_{12}\lambda^3+\delta_{13}\lambda^2+\delta_{14}\lambda+\delta_{15}=0, \tag{6}$$

where

$$\begin{cases}\delta_{11}=-a+b+c+d,\\ \delta_{12}=(e^3+cde^2+bde^2+bce^2-ade^2-ace^2-abe^2-s^2)/e^2,\\ \delta_{13}=(as^2+be^3+ce^3+de^3+bcde^2-ds^2-abce^2\\ \quad -abde^2-acde^2)/e^2,\\ \delta_{14}=(bce^3+bde^3+cde^3+ads^2-es^2-abcde^2)/e^2,\\ \delta_{15}=d(bce^2-s^2)/e.\end{cases} \tag{7}$$

Applying the Routh-Hurwitz conditions, Eq. (6) has all roots with negative real parts if and only if

$$\begin{cases}\delta_{1i}>0,\quad i=1,2,...,5,\\ (\delta_{11}\delta_{14}-\delta_{15})(\delta_{11}\delta_{12}\delta_{13}-\delta_{13}^2-\delta_{11}^2\delta_{14})\\ \quad >\delta_{15}(\delta_{11}\delta_{12}-\delta_{13})^2+\delta_{11}\delta_{15}^2,\\ \delta_{11}\delta_{12}\delta_{13}>\delta_{13}^2+\delta_{11}^2\delta_{14}.\end{cases} \tag{8}$$

The characteristic equation of system (2) evaluated at the equilibrium point E_2 is expressed as

$$\lambda^5+\delta_{21}\lambda^4+\delta_{22}\lambda^3+\delta_{23}\lambda^2+\delta_{24}\lambda+\delta_{25}=0, \tag{9}$$

where

$$\begin{cases}\delta_{21}=-a+b+c+d,\\ \delta_{22}=(s^6+cde^2s^4+c^2e^2s^4+c^2e^5s^4+c^3de^4s^2+b^2c^2e^4s^2\\ \quad +b^2c^4e^6-abc^2e^4s^2-ac^3e^4s^2-adc^2e^4s^2\\ \quad -2bc^3e^4s^2-2bce^2s^4)/(e^4s^2c^2),\\ \delta_{23}=(2ce^6+2dc^2e^2s^4+dc^2e^5s^2+c^3e^5s^2+bc^2e^5s^2\\ \quad +db^2c^2e^4s^2+db^2c^4e^6+2b^3c^4e^6+ds^6-adc^3e^4s^2\\ \quad -2b^2c^3e^4s^2-3bdc^3e^4s^2-acde^2s^4-2bc^2e^2s^4\\ \quad -2bcde^2s^4)/(e^4s^2c^2),\\ \delta_{24}=d(b^3c^3e^6+abc^2e^4s^2+b^2c^2e^4s^2+c^2e^5s^2+3s^6\\ \quad -ace^2s^4-5bce^2s^4+e^3s^4)/(ce^4s^2),\\ \delta_{25}=d(s^2-bce^2)/e.\end{cases} \tag{10}$$

Based on the Routh-Hurwitz conditions, Eq. (9) has all roots with negative real parts if and only if

$$\begin{cases}\delta_{2i}>0,\quad i=1,2,...,5,\\ (\delta_{21}\delta_{24}-\delta_{25})(\delta_{21}\delta_{22}\delta_{23}-\delta_{23}^2-\delta_{21}^2\delta_{24})\\ \quad >\delta_{25}(\delta_{21}\delta_{22}-\delta_{23})^2+\delta_{21}\delta_{25}^2,\\ \delta_{21}\delta_{22}\delta_{23}>\delta_{23}^2+\delta_{21}^2\delta_{24}.\end{cases} \tag{11}$$

For simplification, we consider only the effects of parameters d and s, and set a=3, b=2.5, c=1.0, e=3.5. For s=0 and d varying from 0.01 to 20, it is noticed that the stability conditions of Eq. (4) are not met, and therefore equilibrium point O is unstable. For d varying from 0.01 to 20 and s varying from 0 to 20, it is found that the stability conditions of Eq. (8) are not met, and therefore equilibrium point E_1 is unstable. When d=4, e=3.5, and s=0.1, the equilibrium points and their eigenvalues are given by

$$\begin{cases}\text{For } O(0,0,0,0,0):\lambda_1=-2.5,\lambda_2=-4.0,\lambda_3=-1.0,\\ \quad \lambda_{4,5}=1.5\pm1.118\,03\text{j};\\ \text{For } E_1(-0.028\,77,0,0,0,-0.085\,71):\lambda_1=-2.500\,54,\\ \quad \lambda_2=-4.0,\ \lambda_3=-0.999\,46,\ \lambda_{4,5}=1.5\pm1.118\,03\text{j};\\ \text{For } E_2(-0.028\,57,87.471\,43,-2.499\,19,78.471\,43,\\ \quad 218.521\,46):\lambda_1=0.001\,81,\lambda_2=-9.010\,71,\\ \quad \lambda_3=-0.278\,57,\lambda_{4,5}=2.393\,73\pm87.625\,77\text{j}.\end{cases} \tag{12}$$

Thus, equilibrium points O and $E_{1,2}$ are saddle focused. By varying d from 0.01 to 20 and s from 0 to 20, the stability boundary of equilibrium point E_2 is plotted in Fig. 1.

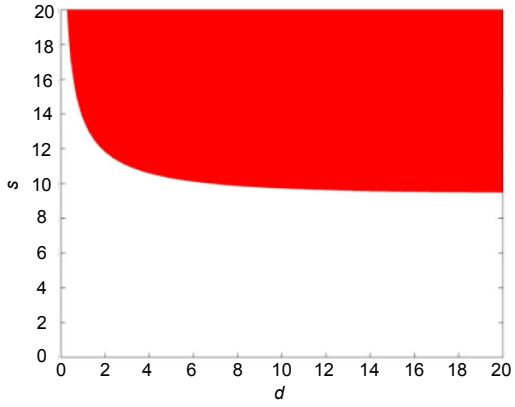

Fig. 1 Stability boundary of equilibrium point E_2
References to color refer to the online version of this figure

In Fig. 1, the red area indicates the region where equilibrium point E_2 is asymptotically stable, while the white region represents the area where the conditions in Eq. (11) are not verified and equilibrium E_2 is unstable. Since equilibrium point E_2 changes the stability properties with different values of d and s, system (2) has either a Hopf or a transcritical bifurcation with different values of d and s.

Setting b=2.5, d=4, and e=3.5, the effects of varying s, c, and a on the dynamical behaviors of system (2) are investigated. Fixing a=3 and c=1, the bifurcation diagrams are plotted in Fig. 2, depicting the local extrema of $x(t)$ and three largest Lyapunov exponents (LLEs).

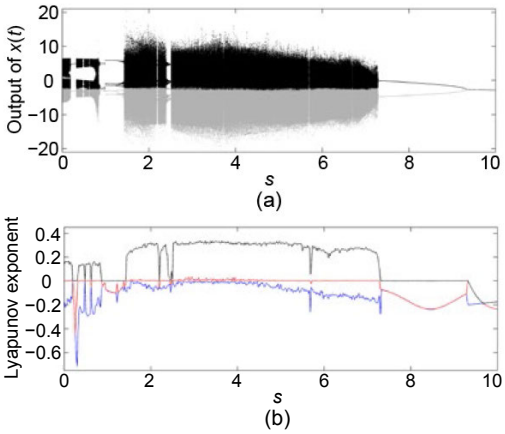

Fig. 2 Bifurcation diagrams depicting the local maxima (black dots) and local minima (gray dots) of $x(t)$ (a) and the three largest Lyapunov exponents (LLEs) (b)
References to color refer to the online version of this figure

By increasing the control parameter s, the dynamics of system (2) presents reverse period-doubling to a chaotic region interspersed with periodic windows (Fig. 2a). By further increasing s, system (2) undergoes a period-1 oscillation observed at s≈9.32, where a Hopf bifurcation occurs followed by the convergence of the trajectories of system (2) to equilibrium point E_2. The dynamical behaviors in Fig. 2a are confirmed by the three LLEs in Fig. 2b. The phase portraits of chaotic oscillations for specific values of parameter s are depicted in Fig. 3.

In Fig. 3, system (2) exhibits two types of chaotic attractors: double-scroll chaotic attractor (Fig. 3a) and one-scroll chaotic attractor (Fig. 3b).

For a=3 and s=0.1, the bifurcation diagrams of $x(t)$ and three LLEs are plotted in Fig. 4.

When c increases from 0.8 to 1.7 (Fig. 4a), the bifurcation diagram of output $x(t)$ shows period-1 oscillations followed by an intermittency route to a chaotic region interspersed with periodic and quasi-periodic windows. The dynamical behaviors in Fig. 4a are confirmed by the three LLEs in Fig. 4b.

For c=1 and s=0.1, the bifurcation diagrams of $x(t)$ and three LLEs are plotted in Fig. 5.

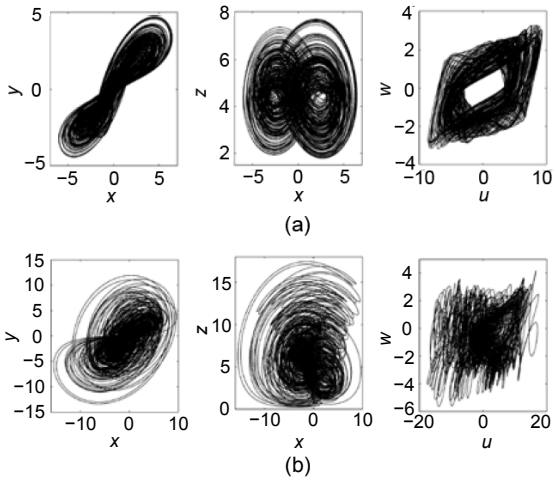

Fig. 3 Projections of chaotic attractors in the x-y, x-z, and u-w planes for s=0.1 (a) and s=2 (b)
a=3, b=2.5, c=1, d=4.0, e=3.5. The initial condition is ($x(0)$, $y(0)$, $z(0)$, $w(0)$, $u(0)$)=(1.0, 1.0, 1.0, 1.0, 1.0)

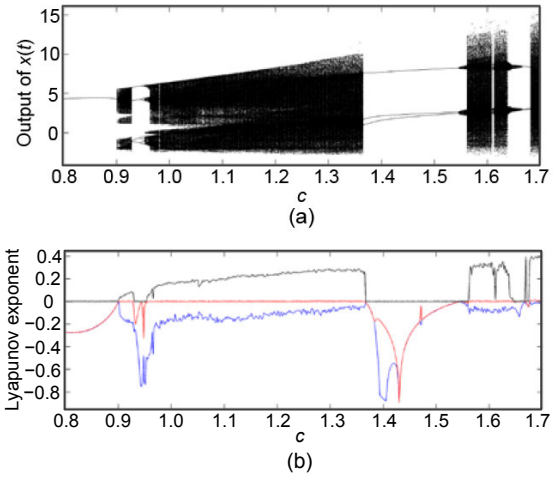

Fig. 4 Bifurcation diagrams depicting the local maxima of $x(t)$ (a) and three largest Lyapunov exponents (LLEs) (b) with a=3, b=2.5, d=4.0, e=3.5, s=0.1

When a varies from 0 to 2.23 (Fig. 5a), the bifurcation diagram of output $x(t)$ exhibits a chaotic region interspersed with periodic windows. By further increasing a, period-2 oscillations are observed for 2.23<a≤2.63 followed by the period-1 oscillations when a≈2.747. Then, another chaotic region interspersed with periodic windows appears for 2.747<a≤3.54, and period-1 oscillations are observed for 3.54<a≤3.71. By ramping a in Figs. 5b and 5c, system (2) displays the same dynamical behaviors as those in Fig. 5a (black dots) in the ranges of 0<a≤2.258 and 2.63<a≤3.71. In the range of

2.258<a≤2.630, system (2) exhibits chaotic behaviors for 2.258≤a≤2.330, period-4 oscillations for 2.320<a<2.400, and period-2 oscillations with large amplitudes compared with the ones in Fig. 5a for 2.400≤a<2.630. From Fig. 5a (black and red dots), one can notice that system (2) displays coexistence of period-2 oscillations and chaotic behaviors in the range of 2.258≤a≤2.320. In the range of 2.320<a<2.400, there is coexistence of period-2 oscillations and period-4 oscillations. In the range of 2.400≤a<2.630, system (2) shows bistable period-2 oscillations. The dynamical behaviors in Fig. 5a in black and red dots are confirmed by the two LLEs in Figs. 5b and 5c, respectively. The coexistence of the attractors and the bistability phenomenon is illustrated in Fig. 6, which depicts the phase portraits of the resulting attractors of system (2) in the x-z plane for different values of a and different initial conditions.

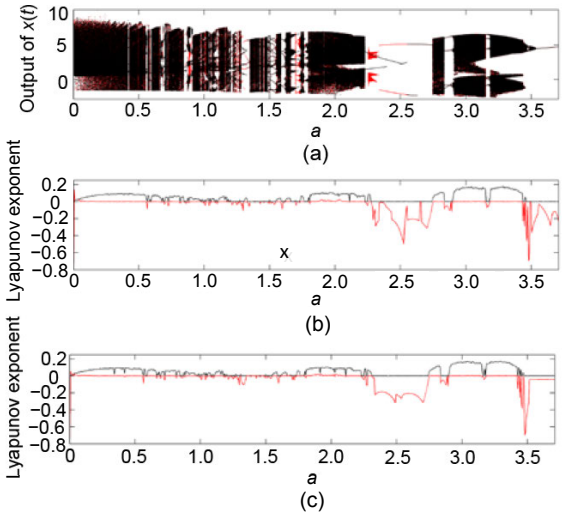

Fig. 5 Bifurcation diagrams depicting the local maxima of $x(t)$ (a) and two LLEs obtained by scanning parameter a upwards (b) and downwards (c) with b=2.5, d=4, e=3.5, s=0.1

References to color refer to the online version of this figure

The coexistence of the chaotic attractor and the period-2 oscillations at a=2.27 is shown in Fig. 6a using the initial conditions of (x(0), y(0), z(0), w(0), u(0))=(1.0, 0, 0.1, 0.1, 0.1) and (x(0), y(0), z(0), w(0), u(0))=(1.0, 1.0, 1.0, 1.0, 1.0). Fig. 6b presents the coexistence of period-2 oscillations and period-4 oscillations for a=2.35 using the initial conditions of (x(0), y(0), z(0), w(0), u(0))=(1.0, 0, 0.1, 0.1, 0.1) and (x(0), y(0), z(0), w(0), u(0))=(1.0, 1.0, 1.0, 1.0, 1.0). In Fig. 6c (gray lines), system (2) displays period-2 oscillations for the initial condition of (x(0), y(0), z(0), w(0), u(0))=(5.0, 1.0, 1.0, 1.0, 1.0). For the initial condition of (x(0), y(0), z(0), w(0), u(0))=(1.0, 1.0, 1.0, 1.0, 1.0), system (2) exhibits period-2 oscillations in Fig. 6c (black lines). Note that extreme multi-stability is not found in system (2), but it exhibits multi-stability as shown in Fig. 6.

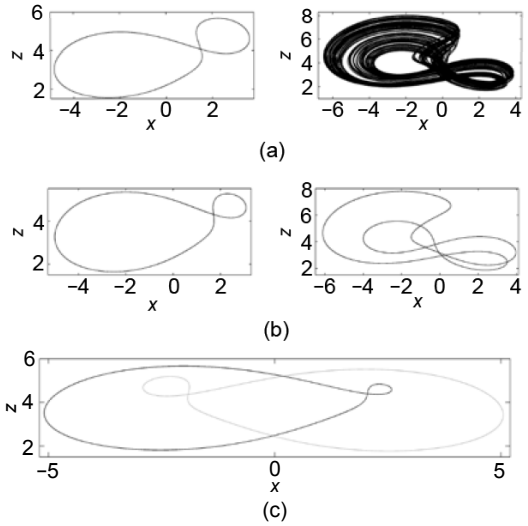

Fig. 6 Coexistence of attractors and bistable attractors in the x-z plane for different values of a and different initial conditions: (a) a=2.27; (b) a=2.35; (c) a=2.45

b=2.5, c=1, d=4.0, e=3.5, s=0.1

The state variable u appears only in the first equation of autonomous system (2), and its amplitude can be changed by inserting a boosting controller γ into system (2), expressed as

$$\begin{cases} \dot{x} = ax - yz - (u + \gamma), \\ \dot{y} = -by + xz - zw, \\ \dot{z} = -cz + xy, \\ \dot{w} = d(y - w), \\ \dot{u} = ex + s. \end{cases} \tag{13}$$

To check the partial amplitude control of chaotic system (13), the phase portraits and time series of state variable u of system (13) are depicted in Fig. 7 with different values of boosting controller γ.

As shown in Fig. 7, for the initial condition of (x(0), y(0), z(0), w(0), u(0))=(1.0, 1.0, 1.0, 1.0, 1.0),

the chaotic signal u is boosted from a bipolar signal to a unipolar signal when decreasing the boosting controller γ.

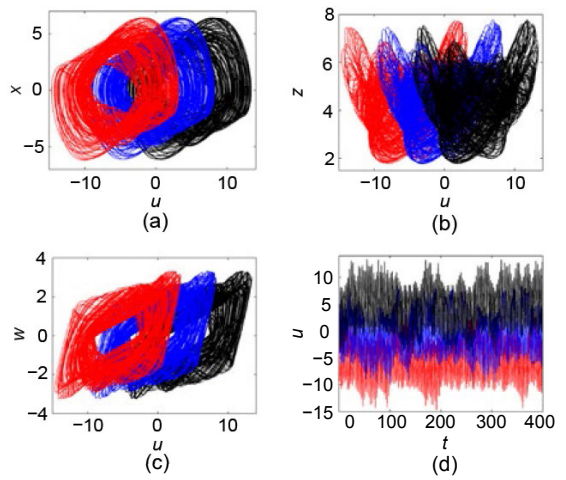

Fig. 7 Phase portraits in the *u*-*x* plane (a), *u*-*z* plane (b), and *u*-*w* plane (c) and time series (d) of signal *u* of system (13) for *a*=3, *b*=2.5, *c*=1, *d*=4.0, *e*=3.5, and *s*=0.1

γ=−4 (black), 1 (blue), and 6 (red). References to color refer to the online version of this figure

3 FPGA implementation of the proposed 5D autonomous system with offset boosting

Some literature has discussed FPGA implementation including FPGA-based multi-scroll chaotic oscillators (Tlelo-Cuautle et al., 2015), four-wing chaotic attractors (Dong et al., 2016), memristor-based chaotic attractors (Xu et al., 2016), image cryptography with chaotic ciphers (Barakat et al., 2011), and an autonomous Jerk oscillator (Rajagopal et al., 2018). Hyperchaotic oscillators with complex mathematical models have been implemented using FPGAs, showing that FPGA is a systematic platform for implementing high-standard, high-throughput approximations to high-order systems that are less costly and require a short time span to design (Rajagopal et al., 2017a, 2017d). Compared with other processors, FPGAs have well fixed hardware for processing logic, and hence their achievement is not influenced by the complexities of the system. Modern versions of FPGAs highlight low dynamic power performance, and therefore they can be used in a progressive manner for many electronic applications (Bahi et al., 2013; Ismail et al., 2017; Woods et al., 2017). The processor-based system has layers of abstraction to schedule tasks and share resources among multiple resources. These compilations are not mandatory for FPGA applications. The proposed autonomous 5D chaotic system is designed using the Hardware Description Language (HDL) coder in the Xilinx system generator. Either VHDL or VERILOG code is generated using the Vivado synthesis tool, which is based on HDL code selection, while configuring the design of the system. FPGA realizations generate intense hardware–software co-simulations when using different parameters under the same conditions (Jiang et al., 2007). The major task in such realization is to determine the type of the numerical method to solve the proposed hyperchaotic system. We choose the forward Euler method to solve the proposed autonomous 5D chaotic system. The set of discretized system equations (Charef, 2006) is given by

$$\begin{cases} x_{k+1} = x_k + h(ax_{k-1} - y_{k-1}z_{k-1} - u_{k-1}), \\ y_{k+1} = y_k + h(-by_{k-1} + x_{k-1}z_{k-1} - z_{k-1}w_{k-1}), \\ z_{k+1} = z_k + h(-cz_{k-1} + x_{k-1}y_{k-1}), \\ w_{k+1} = w_k + h(dy_{k-1} - dw_{k-1}), \\ u_{k+1} = u_k + h(ex_{k-1} + s), \end{cases} \tag{14}$$

where a, b, c, d, e, and s are the system parameters and h the step size of the discrete numerical solution. The discrete state equation of the proposed autonomous 5D chaotic system is implemented on the FPGA in discrete time (Chen YQ et al., 2004; Rajagopal et al., 2017b), and the required basic arithmetic operators are implemented using the XSG tool box in Simulink (Wang QX et al, 2016). We configure the available built-in blocks of the system generator tool box such as the Add/Sub and multiplier blocks with zero latency and use 32/16-bit fixed point settings (according to the IEEE 754 Standard). The output of the block is configured to rounded quantization to reduce the bit latency. In particular, the integrator block is designed using the mathematical relationship, i.e., $\mathrm{d}x_i/\mathrm{d}t = \lim_{h\to 0}[x_i(n+1) - x_i(n)]/h$. To attain accuracy, we select h=0.001 and the initial conditions required for the proposed autonomous 5D chaotic system are fed into the forward register of the integrator block designed using Euler's formula. Fig. 8 shows the Xilinx register-transfer level (RTL) schematic of the proposed chaotic system using the Kintex-7 chip.

Figs. 9–12 show the phase portraits of the proposed autonomous 5D chaotic system using the Xilinx system generator.

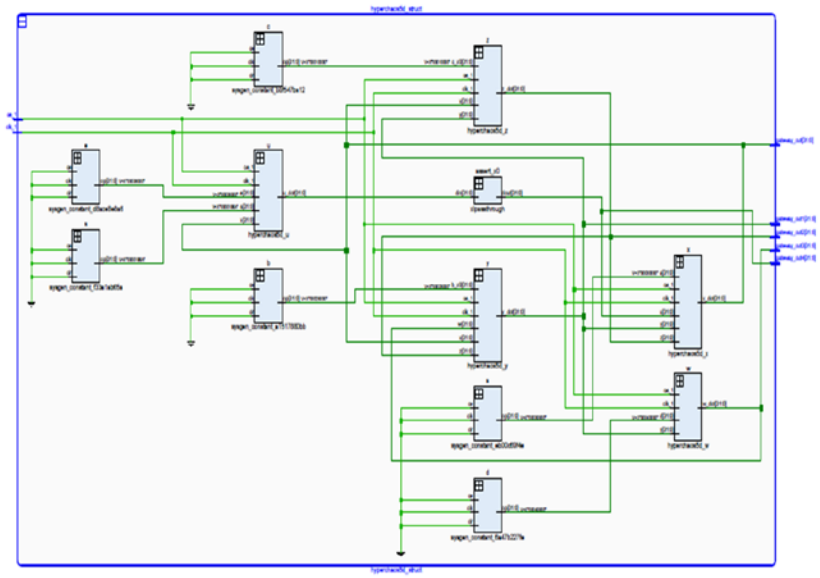

Fig. 8 Register-transfer level schematic of the proposed autonomous 5D system (13) implemented by the Kintex-7 chip

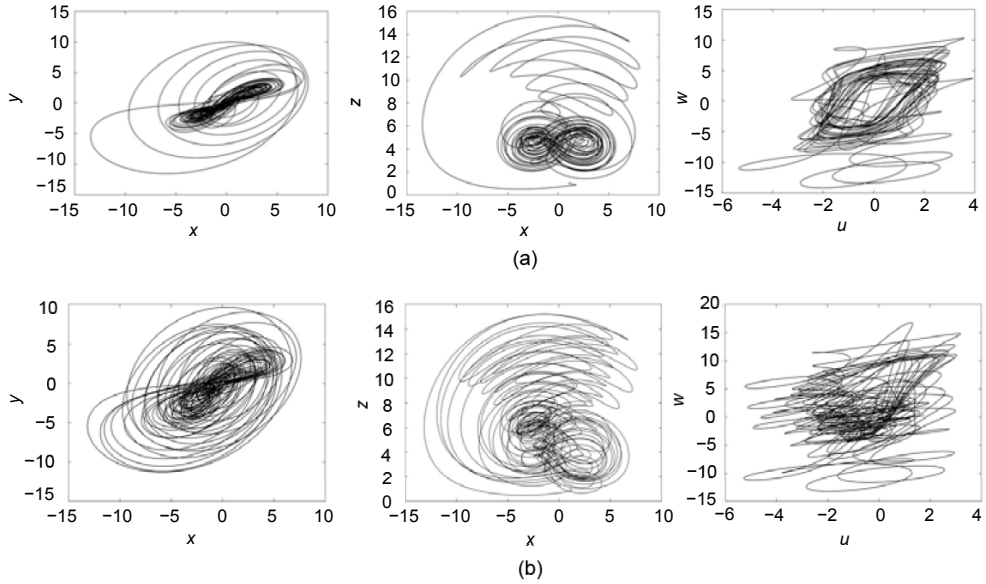

Fig. 9 Phase portraits in the *x*-*y*, *x*-*z*, and *u*-*w* planes of the proposed FPGA-implemented autonomous 5D system with hardware–software co-simulation for *s*=0.1 (a) and *s*=2 (b)
a=3, *b*=2.5, *d*=4.0, *e*=3.5, *γ*=0. The initial condition is [1.0, 1.0, 1.0, 1.0, 1.0]

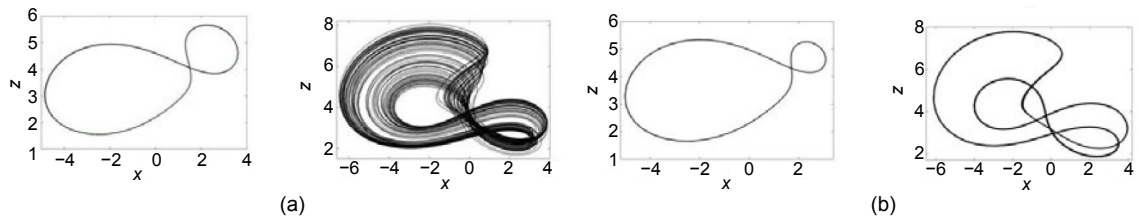

Fig. 10 Phase portraits showing coexisting attractors in the *x*-*z* plane of the proposed FPGA-implemented autonomous 5D system for different values of *a* and different initial conditions: (a) *a*=2.27; (b) *a*=2.35
In the left panel of (a) and (b), the initial condition is ($x(0)$, $y(0)$, $z(0)$, $w(0)$, $u(0)$)=(1.0, 0, 0.1, 0.1, 0.1), while in the right panel the initial condition is ($x(0)$, $y(0)$, $z(0)$, $w(0)$, $u(0)$)=(1.0, 1.0, 1.0, 1.0, 1.0). *b*=2.5, *d*=4.0, *c*=1, *e*=3.5, *s*=0.1, *γ*=0

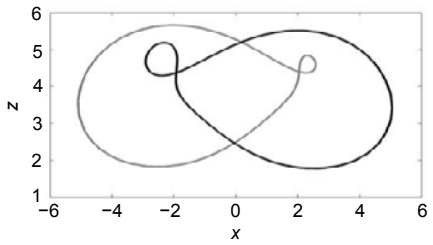

Fig. 11 Phase portrait showing the bistable attractors in the *x*-*z* plane of the proposed FPGA-implemented autonomous 5D system for *a*=2.45

Black curves are obtained using the initial condition of ($x(0)$, $y(0)$, $z(0)$, $w(0)$, $u(0)$)=(5.0, 1.0, 1.0, 1.0, 1.0), and gray curves are obtained using the initial condition of ($x(0)$, $y(0)$, $z(0)$, $w(0)$, $u(0)$)=(1.0, 1.0, 1.0, 1.0, 1.0). b=2.5, c=1, d=4.0, e=3.5, s=0.1, γ=0

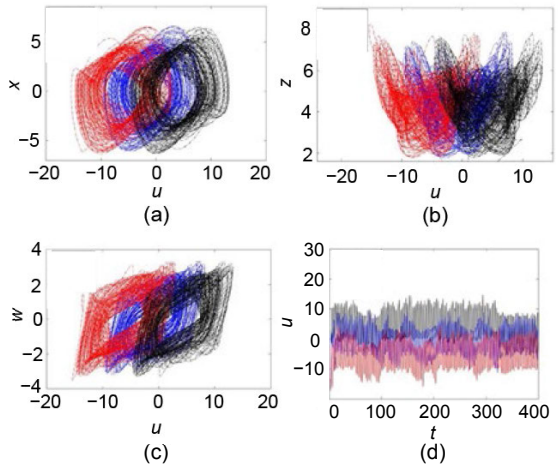

Fig. 12 Phase portraits in the *u*-*x* plane (a), *u*-*z* plane (b), *u*-*w* plane (c), and time series of signal *u* of system (13) (d) of the proposed FPGA-implemented autonomous 5D system for *a*=3.0, *b*=2.5, *c*=1.0, *d*=4.0, *e*=3.5, *s*=0.1

γ=−4 (black), 1 (blue), and 6 (red). The initial condition is [1.0, 1.0, 1.0, 1.0, 1.0]. References to color refer to the online version of this figure

4 Sound encryption using the proposed autonomous 5D system with offset boosting

Multimedia security has attracted a lot of attention because of its importance in various applications, such as e-education and the military use, and leads to the importance of real-time and sufficiently secure and robust image encryption methods (Azarang et al., 2017; Li CQ et al., 2018b, 2019; Li XW et al., 2019). In this section, a sound encryption and communication system using the proposed autonomous 5D chaotic system (2) is designed and analyzed by the MATLAB Simulink software. The system consists of a transmitter and a receiver unit. The MATLAB Simulink block diagram of the transmitter unit is shown in Fig. 13.

In the transmitter unit, sound signal $m(t)$ is converted to binary number data. To encrypt the sound signal, the y state variable output $C_y(t)$ of the proposed autonomous 5D chaotic system (2) is used. In the floating-to-binary unit in Fig. 13, the y state variable value is converted to 64-bit floating point number format and the 2nd bit value of the floating point number value is sent to the output. The EXOR operation is applied to the value of the floating-to-binary unit output and the binary data value of the sound signal. Data coming from the EXOR unit is compared in the threshold detector unit. The output of the threshold detector unit is "1" if the incoming data is "1" and "−1" if the incoming data is "0." With this algorithm, the sound signal is encrypted using the y state variable value of chaotic system (2). The encrypted sound signal $e(t)$ obtained is summed with the x state variable output $C_x(t)$ of the proposed autonomous 5D chaotic system (2). Thus, the encrypted

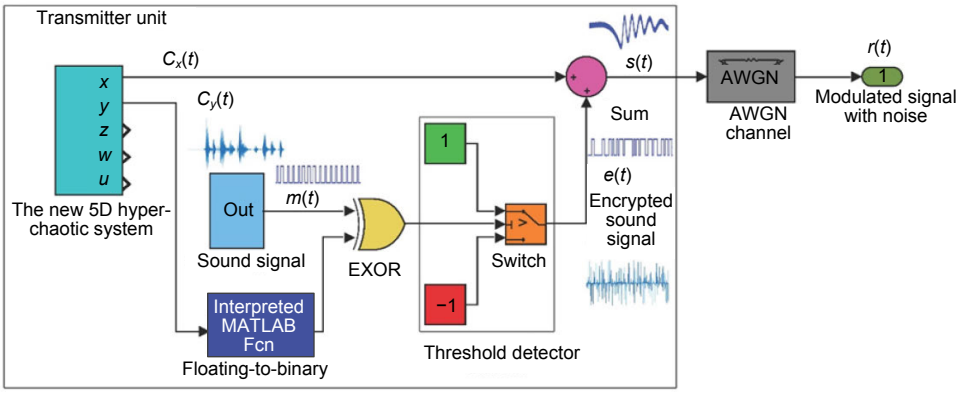

Fig. 13 MATLAB Simulink block diagram of the transmitter unit

sound signal is masked by the chaotic signal. In this way, the previously encrypted sound signal is again encrypted by the masked chaotic signal $C_x(t)$, and the obtained modulated signal $s(t)$ is sent to the transmission medium. As a result, the sound signals are sent more securely to the communication medium. The additive white Gaussian noise (AWGN) channel model is used as a noise source in the system analysis. Thus, a modulated signal with noise $r(t)$ can be obtained in the system. The MATLAB Simulink block diagram of the receiver unit is shown in Fig. 14.

At the receiver unit, the x state variable output $C_x(t)$ of the proposed autonomous 5D chaotic system (2) is subtracted from the incoming noisy modulated signal $r(t)$. The signal obtained through this process is quantized to be 0 or 1 in the threshold detector. Thus, the encrypted sound signal is obtained from the noisy chaotic modulated signal $r(t)$ coming from the transmitting unit in the communication medium. In the floating-to-binary unit in Fig. 14, as in the transmitter unit, the y chaotic signal $C_y(t)$ is converted to the 64-bit floating point number format and the 2nd bit value of the floating point number value is sent to the output. The EXOR operation is applied to the value of the floating-to-binary unit output and the threshold detector unit output. In this way, the encryption of the encrypted sound signal is resolved and the original sound signal $\sim m(t)$ sent from the transmitting unit is obtained. The sound encryption and communication system is analyzed under the AWGN channel noise model varying from 0- to 10-dB E_b/N_0 (energy per bit to noise density) in MATLAB Simulink. For the sound signal to be used for testing purposes, a two-second sound recording from the microphone at a sample rate of 8 kHz is used. The bit-error-rate (BER) performance of the system is shown in Fig. 15.

Fig. 16 shows the transmitted sound signal data, encrypted sound signal data, and sound signal data obtained from the test results of the designed system at a 100 kHz communication speed under 10-dB E_b/N_0. The transmitted encrypted sound signal is successfully obtained in the receiver unit.

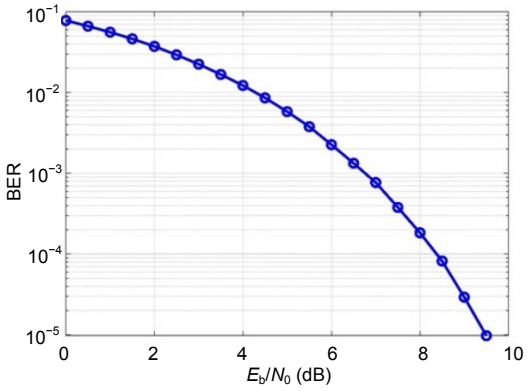

Fig. 15 Bit-error-rate (BER) performance of the system

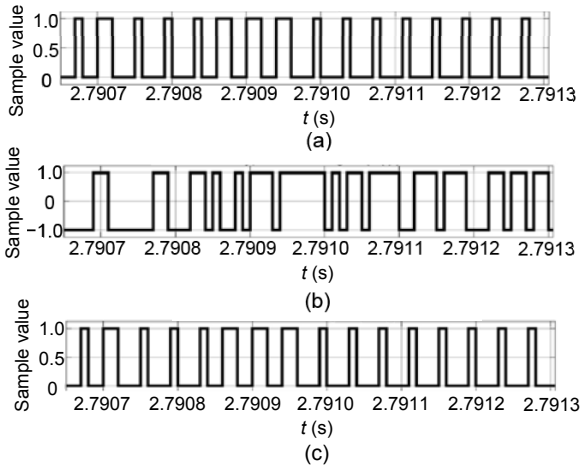

Fig. 16 Signal data obtained from system (2): (a) transmitted sound signal $m(t)$; (b) encrypted sound signal $e(t)$; (c) obtained sound signal $\sim m(t)$

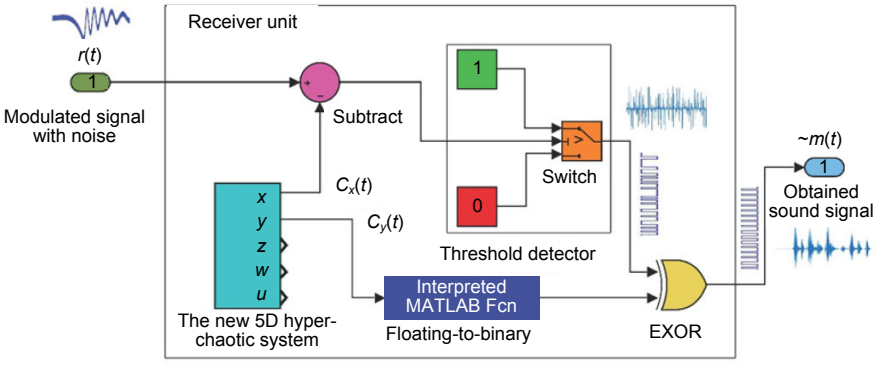

Fig. 14 MATLAB Simulink block diagram of the receiver unit

Fig. 17 shows the transmitted original sound signal, encrypted sound signal, chaos-based modulated signal with noise sent by the transmitter unit to the transmission medium, and sound signal obtained by the receiver unit.

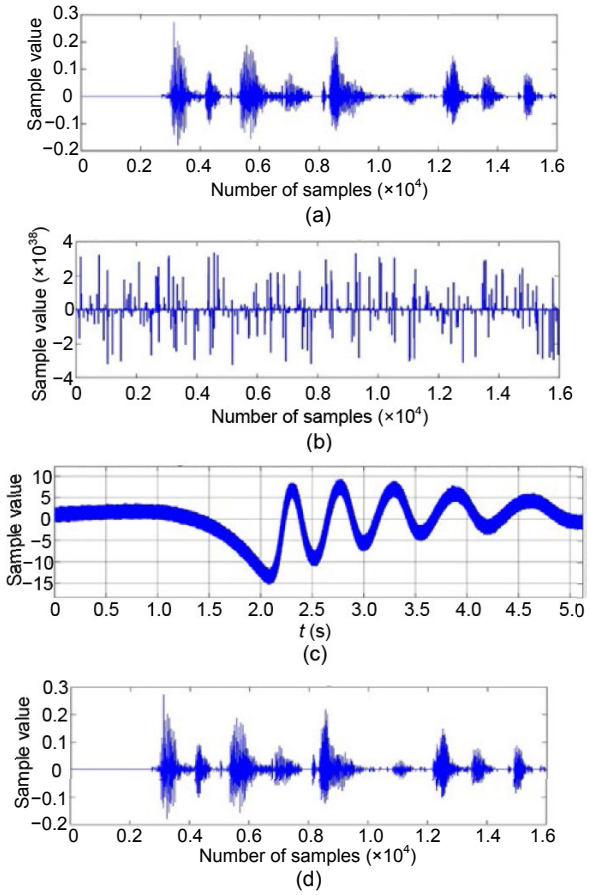

Fig. 17 Transmitted sound signal (a), encrypted sound signal (b), modulated signal (c) sent to the communication medium with noise, and the obtained sound signal (d)

5 Conclusions

In this study, we analyzed the FPGA implementation of an autonomous five-dimensional (5D) system with offset boosting and its application to a sound encryption scheme using a chaos masking technique. The proposed autonomous 5D system was investigated analytically and numerically. It was found that the proposed system displays several interesting features and behaviors, including Hopf bifurcation, reverse period-doubling route to chaos, intermittency route to chaos, bistability phenomenon, periodic, quasi-periodic, and one- and double-scroll chaotic attractors, and partial amplitude control of its signals. The proposed autonomous 5D system was implemented using FPGA to show that it can be realized in hardware. Finally, the chaotic behavior of the proposed autonomous 5D system was used to design and implement a sound encryption scheme using the MATLAB Simulink software.

Contributors

Sifeu TAKOUGANG KINGNI developed the model and analyzed the data. Karthikeyan RAJAGOPAL performed the FPGA implementation. Serdar ÇIÇEK developed the sound encryption application. Ashokkumar SRINIVASAN and Anitha KARTHIKEYAN participated in the data analysis and FPGA implementation at different stages, and helped organize the manuscript. All authors contributed to the interpretation of the results. Sifeu TAKOUGANG KINGNI, Karthikeyan RAJAGOPAL, and Serdar ÇIÇEK drafted the manuscript. Sifeu TAKOUGANG KINGNI revised and finalized the paper.

Compliance with ethics guidelines

Sifeu TAKOUGANG KINGNI, Karthikeyan RAJAGOPAL, Serdar ÇIÇEK, Ashokkumar SRINIVASAN, and Anitha KARTHIKEYAN declare that they have no conflict of interest.

References

Azarang A, Ranjbar J, Mohseni H, et al., 2017. Output feedback synchronization of a novel chaotic system and its application in secure communication. *Int J Comput Sci Netw Secur*, 17:72-77.

Bahi JM, Fang XL, Guyeux C, et al., 2013. FPGA design for pseudorandom number generator based on chaotic iteration used in information hiding application. *Appl Math Inform Sci*, 7(6):2175-2188. https://doi.org/10.12785/amis/070607

Barakat ML, Radwan AG, Salama KN, 2011. Hardware realization of chaos based block cipher for image encryption. Int Conf on Microelectronics. https://doi.org/10.1109/ICM.2011.6177386

Charef A, 2006. Analogue realisation of fractional-order integrator, differentiator and fractional $PI^{\lambda}D^{\mu}$ controller. *IEEE Proc Contr Theory Appl*, 153(6):714-720. https://doi.org/10.1049/ip-cta:20050019

Chen YM, Yang QG, 2015. A new Lorenz-type hyperchaotic system with a curve of equilibria. *Math Comput Simul*, 112:40-55. https://doi.org/10.1016/j.matcom.2014.11.006

Chen YQ, Vinagre BM, Podlubny I, 2004. Continued fraction expansion approaches to discretizing fractional order derivatives—an expository review. *Nonl Dynam*, 38(1-4): 155-170. https://doi.org/10.1007/s11071-004-3752-x

Dong EZ, Liang ZH, Du SZ, et al., 2016. Topological horseshoe analysis on a four-wing chaotic attractor and its FPGA implement. *Nonl Dynam*, 83(1-2):623-630. https://doi.org/10.1007/s11071-015-2352-2

Hou YY, Chen HC, Chang JF, et al., 2012. Design and implementation of the Sprott chaotic secure digital communication systems. *Appl Math Comput*, 218(24): 11799-11805. https://doi.org/10.1016/j.amc.2012.04.076

Hu G, 2009. Generating hyperchaotic attractors with three positive Lyapunov exponents via state feedback control. *Int J Bifurc Chaos*, 19(2):651-660. https://doi.org/10.1142/S0218127409023275

Ismail SM, Said LA, Rezk AA, et al., 2017. Generalized fractional logistic map encryption system based on FPGA. *Int J Electron Commun*, 80:114-126. https://doi.org/10.1016/j.aeue.2017.05.047

Jia Q, 2007. Projective synchronization of a new hyperchaotic Lorenz system. *Phys Lett A*, 370(1):40-45. https://doi.org/10.1016/j.physleta.2007.05.028

Jiang CX, Carletta JE, Hartley TT, 2007. Implementation of fractional-order operators on field programmable gate arrays. In: Sabatier J, Agrawal OP, Tenreiro JA (Eds.), Machado Advances in Fractional Calculus: Theoretical Developments and Applications in Physics and Engineering. Springer, Dordrecht, the Netherlands, p.333-346. https://doi.org/10.1007/978-1-4020-6042-7_23

Li CQ, Lin DD, Feng BB, et al., 2018a. Cryptanalysis of a chaotic image encryption algorithm based on information entropy. *IEEE Access*, 6:75834-75841. https://doi.org/10.1109/ACCESS.2018.2883690

Li CQ, Lin DD, Lü JH, et al., 2018b. Cryptanalyzing an image encryption algorithm based on autoblocking and electrocardiography. *IEEE Multim*, 25(4):46-56. https://doi.org/10.1109/MMUL.2018.2873472

Li CQ, Feng BB, Li SJ, et al., 2019. Dynamic analysis of digital chaotic maps via state-mapping networks. *IEEE Trans Circ Syst I*, 66(6):2322-2335. https://doi.org/10.1109/TCSI.2018.2888688

Li QD, Zeng HZ, Li J, 2015. Hyperchaos in a 4D memristive circuit with infinitely many stable equilibria. *Nonl Dynam*, 79(4):2295-2308. https://doi.org/10.1007/s11071-014-1812-4

Li X, 2009. Modified projective synchronization of a new hyperchaotic system via nonlinear control. *Commun Theor Phys*, 52(2):274-278. https://doi.org/10.1088/0253-6102/52/2/17

Li XW, Wanga Y, Wang QH, et al., 2019. Modified integral imaging reconstruction and encryption using an improved SR reconstruction algorithm. *Opt Laser Eng*, 112:162-169. https://doi.org/10.1016/j.optlaseng.2018.09.015

Li YX, Chen GR, Tang WKS, 2005. Controlling a unified chaotic system to hyperchaotic. *IEEE Trans Circ Syst II*, 52(4):204-207. https://doi.org/10.1109/TCSII.2004.842413

Liu WB, Chen GR, 2004. Dynamical analysis of a chaotic system with two double-scroll chaotic attractors. *Int J Bifurc Chaos*, 14(3):971-998. https://doi.org/10.1142/S0218127404009715

Lorenz EN, 1963. Deterministic nonperiodic flow. *J Atmos Sci*, 20(2):130-141. https://doi.org/10.1175/1520-0469(1963)020<0130:DNF>2.0.CO;2

Ojoniyi OS, Njah AN, 2016. A 5D hyperchaotic Sprott B system with coexisting hidden attractors. *Chaos Sol Fract*, 87:172-181. https://doi.org/10.1016/j.chaos.2016.04.004

Qi GY, van Wyk MA, van Wyk BJ, et al., 2008. On a new hyperchaotic system. *Phys Lett A*, 372(2):124-136. https://doi.org/10.1016/j.physleta.2007.10.082

Rajagopal K, Guessas L, Vaidyanathan S, et al., 2017a. Dynamical analysis and FPGA implementation of a novel hyperchaotic system and its synchronization using adaptive sliding mode control and genetically optimized PID control. *Math Probl Eng*, 2017:7307452. https://doi.org/10.1155/2017/7307452

Rajagopal K, Karthikeyan A, Srinivasan AK, 2017b. FPGA implementation of novel fractional-order chaotic systems with two equilibriums and no equilibrium and its adaptive sliding mode synchronization. *Nonl Dynam*, 87(4):2281-2304. https://doi.org/10.1007/s11071-016-3189-z

Rajagopal K, Guessas L, Karthikeyan A, et al., 2017c. Fractional order memristor no equilibrium chaotic system with its adaptive sliding mode synchronization and genetically optimized fractional order PID synchronization. *Complexity*, 2017:1892618. https://doi.org/10.1155/2017/1892618

Rajagopal K, Karthikeyan A, Duraisamy P, 2017d. Hyperchaotic chameleon: fractional order FPGA implementation. *Complexity*, 2017:8979408. https://doi.org/10.1155/2017/8979408

Rajagopal K, Kingni ST, Kuiate GF, et al., 2018. Autonomous Jerk oscillator with cosine hyperbolic nonlinearity: analysis, FPGA implementation, and synchronization. *Adv Math Phys*, 2018:7273531. https://doi.org/10.1155/2018/7273531

Rech PC, 2014. Delimiting hyperchaotic regions in parameter planes of a 5D continuous-time dynamical system. *Appl Math Comput*, 247:13-17. https://doi.org/10.1016/j.amc.2014.08.084

Rössler OE, 1979. An equation for hyperchaos. *Phys Lett A*, 71(2-3):155-157. https://doi.org/10.1016/0375-9601(79)90150-6

Shen CW, Yu SM, Lü JH, et al., 2014. A systematic methodology for constructing hyperchaotic systems with multiple positive Lyapunov exponents and circuit implementation. *IEEE Trans Circ Syst I*, 61(3):854-864. https://doi.org/10.1109/TCSI.2013.2283994

Singh JP, Rajagopal K, Roy BK, 2018. A new 5D hyperchaotic system with stable equilibrium point, transient chaotic behaviour and its fractional-order form. *Pramana*, 91(3): 33. https://doi.org/10.1007/s12043-018-1599-9

Thamilmaran K, Lakshmanan M, Venkatesan A, 2004. Hyperchaos in a modified canonical Chua's circuit. *Int J Bifurc Chaos*, 14(1):221-243. https://doi.org/10.1142/S0218127404009119

Tlelo-Cuautle E, Rangel-Magdaleno JJ, Pano-Azucena AD, et al., 2015. FPGA realization of multi-scroll chaotic oscillators. *Commun Nonl Sci Numer Simul*, 27(1-3):66-80.

https://doi.org/10.1016/j.cnsns.2015.03.003

Vaidyanathan S, 2013. A ten-term novel 4-D hyperchaotic system with three quadratic nonlinearities and its control. *Int J Contr Theory Appl*, 6(2):97-109.

Wang JH, Chen ZQ, Chen GR, et al., 2008. A novel hyperchaotic system and its complex dynamics. *Int J Bifurc Chaos*, 18(11):3309-3324. https://doi.org/10.1142/S0218127408022391

Wang QX, Yu SM, Li CQ, et al., 2016. Theoretical design and FPGA-based implementation of higher-dimensional digital chaotic systems. *IEEE Trans Circ Syst I*, 63(3):401-412. https://doi.org/10.1109/TCSI.2016.2515398

Wang XY, Wang MJ, 2008. A hyperchaos generated from Lorenz system. *Phys A*, 387(14):3751-3758. https://doi.org/10.1016/j.physa.2008.02.020

Wei ZC, Moroz I, Sprott JC, et al., 2017. Hidden hyperchaos and electronic circuit application in a 5D self-exciting homopolar disc dynamo. *Chaos*, 27:033101. https://doi.org/10.1063/1.4977417

Wei ZC, Rajagopal K, Zhang W, et al., 2018. Synchronisation, electronic circuit implementation, and fractional-order analysis of 5D ordinary differential equations with hidden hyperchaotic attractors. *Pramana*, 90(4):50. https://doi.org/10.1007/s12043-018-1540-2

Woods R, McAllister J, Yi Y, et al., 2017. FPGA-Based Implementation of Signal Processing Systems. Wiley, Chichester, UK.

Xu YM, Wang LD, Duan SK, 2016. A memristor-based chaotic system and its field programmable gate array implementation. *Acta Phys Sin*, 65(12):120503 (in Chinese). https://doi.org/10.7498/aps.65.120503

Yang QG, Chen CT, 2013. A 5D hyperchaotic system with three positive Lyapunov exponents coined. *Int J Bifurc Chaos*, 23(6):1350109. https://doi.org/10.1142/S0218127413501095

Yang QG, Liu YJ, 2009. A hyperchaotic system from a chaotic system with one saddle and two stable node-foci. *J Math Anal Appl*, 360(1):293-306. https://doi.org/10.1016/j.jmaa.2009.06.051

Yang QG, Zhang KM, Chen GR, 2009. Hyperchaotic attractors from a linearly controlled Lorenz system. *Nonl Anal Real World Appl*, 10(3):1601-1617. https://doi.org/10.1016/j.nonrwa.2008.02.008